ORIGINAL PAPER

Sensitive competitive label-free electrochemical immunosensor for primal detection of ovarian cancer

Saima Rafique[1] · **Sobia Tabassum**[2] · **Rizwan Akram**[1]

Abstract

A simple, sensitive and one-step electrochemical technique was employed for the development of sandwich electrochemical immunosensor for the detection of CA 125 antigen. A unique three-dimensional gold nanostructure grown substrate is developed by electrodeposition technique to immobilize a large amount of anti-CA 125 through functionalization of gold nanostructures to immobilize cancer biomarker CA 125 and in human serum as well. The prepared immunosensor can directly amplify the electrochemical signal by making use of silicon nanoparticles conjugated with target antibody to achieve a detection limit of 1 pg ml^{-1} in human serum. However, a comparative low detection limit of 1 fg ml^{-1} with wide dynamic range from 1 μg ml^{-1} to 1 fg ml^{-1} was obtained in cancer biomarker CA 125 solution. The immunosensor is sensitive, stable and reproducible in clinical serum samples. This gold nanostructures-based sandwich immunosensor can be mass manufactured, which may offer great potential to fabricate economical and sensitive immunosensor for broad applications in clinical diagnosis.

Keywords Gold nanostructures · Electrodeposition · Sandwich immunosensor · Electrochemical biomarker detection

Introduction

The unusual growth of abnormal cells in ovary initiated to form a tumor known as ovarian cancer (OC). In women, this is the eighth most commonly occurring cancer and worldwide 18th most common cancer worldwide. In 2018, approximately 300,000 new cases appeared from all over the world (Bray et al. 2018). In Pakistan, according to the Globocan statistics 2018, OC is ranked 10th and, out of 92,639 cancer cases 4504 cases were of OC (World Health Organization 2019). The average lifetime risk of developing OC is 1.35%. The highest risk of OC is associated with menopausal hormone therapy (MHT), whereas the lowest risk is with oral contraceptives usage, malnutrition and oophorectomy (Torre et al. 2018).

Surgery, chemotherapy, radiation, hormonal or targeted therapy can be adopted as treatment of OC depending on its stage. Most commonly, platinum and texane combination therapy approach is implemented for first-line chemotherapy (Orr and Edwards 2018). Recent research focuses on more targeted therapy to reduce the risk of damaging or killing the normal cells. The angiogenesis inhibitors (bevacizumab) that binds to VEGF receptors and the PARP inhibitors (olaparib, rucaparib, and niraparib) are the conventional drugs for *BRCA* mutant patients that are being implemented as best targeted therapy [PDQ Adult Treatment Editorial Board (2019). However, the common side effects are nausea, high blood pressure, low white blood cell counts, anemia, fatigue, bleeding, loss of appetite, diarrhea, muscle and joint pain (Kim et al. 2017). The success of these chemotherapeutics is also limited due to inherent and acquired resistance of cancer cells. The efficiency of these drugs can be increased by development of novel nanocarriers which promise more targeted therapy, improves tissue uptake, bioavailability, and pharmacokinetics of present chemotherapeutic agents (Cheng et al. 2018). For example Schumann et al. (2015) have developed the polypropylenimine dendrimer-based nanoparticles for effective DJ-1 protein knockdown for platinum-resistant OC. Most recently, chitosan nanoformulations

✉ Saima Rafique
saima.rafique@mail.au.edu.pk

1 Department of Physics, Air University, PAF Complex, E-9, Islamabad 44000, Pakistan

2 Department of Bioinformatics and Biotechnology, International Islamic University, H-10 Campus, Islamabad, Pakistan

and modifications have been applied for delivery of therapeutic agents to the cancerous ovarian cells for improving treatment effects (Alizadeh et al. 2019). The patients suffering from OC have low survival rates with the majority of patients diagnosed with either stage 3 or 4 having 5-year survival rate of 27% and 16%, respectively. So, together with the advancement in therapeutic efficiency, improvement in prognosis of OC is essential in early stages (Dochez et al. 2019). In 1976, carcinoembryonic antigen (CEA) was described as a first blood test for women with ovarian cancer. But lately, cancer antigen 125 (CA-125) was announced as more potential biomarker for OC specifically. CA-125 is a remarkably large protein of 200–2000 kDa weight due to highly variable glycosylation. It is also known as mucin 16 or MUC16 that is encoded by the MUC16 gene in humans. The Food and Development Administration (FDA) has never approved CA125 for detection of OC in the United States. Most of CA125 tests are for the evaluation of OC before surgery. Also, the usage of CA125 serum has never been related with a decent survival rate. Twenty-five years after its discovery, it has been recommended for clinical use for OC screening of high-risk OC patients (Ueland et al. 2017; Scholler and Urban 2007). Presently, only 25% patients are diagnosed positively for stage 1 or 2 OC disease, which is not much promising. Besides, current OC diagnosis also requires frequent ultrasonography screenings for observing variations in the ovaries of patients. Even then, current diagnostic techniques are not considered conclusive without the patient's CA125 level analysis (Menon et al. 2009; www.cancerresearchuk.org; Gazze et al. 2018). Furthermore, the serum CA125 assay has low sensitivity in the early stages (Dochez et al. 2019), therefore research should be focused on development of CA125 as a true diagnostic test with its highly sensitive biomarker property.

Nanoparticles have remarkable diagnostic and imaging property for cancer. This is because metal nanostructures (Jeyaraj et al. 2013a, b; Jeyaraj et al. 2013a, b), carbon-based nanoparticles, polymer hybrid nanometerials (Mehnath et al. 2018) and quantum dots functionalized by an antibody can be implied to detect molecular marker present on the surface of cancer cells (Paris and María 2018). With advancement in nanomaterial research, diagnosis and treatment of OC has improved, such as their use in fluorescence image-guided surgery and ultrasound responsive nanoparticles (Lorenzo et al. 2018). Due to the remarkable properties of gold in imaging and as diagnosis (Singh et al. 2018), the gold nanostructure can be coupled with immunosensor CA125 to develop a more sensitive and economical biosensor.

In this paper, an electrochemical immunosensor based on one-step electrodeposition of three-dimensional gold nanostructures (GNS) was developed for ovarian cancer detection, which can be used for primal cancer diagnosis. The immunosensor was synthesized on plane and GNS electrodes. It is observed that GNS have better electrochemical performance compared to plane Au electrode. Therefore, the GNS electrode was used for detection of CA125 antigen. Thereafter, silicon nanoparticles (SiNPs) conjugated with target antibody was used to synthesize sandwich immunosensor, which enhanced the antibody loading and enhanced the sensitivity towards antigen detection. Electrochemical impedance spectroscopy was used to study the effect of GNS electrode for detection of CA125 antigen. We explored how nanostructuring and sandwiching influenced the sensitivity of immunosensor which can determine the lower limit of detection.

Experimental section

Materials

The chemicals used in experiments were of analytical grade. Hydrogen tetrachloroaurate (III) trihydrate ($HAuCl_4 \cdot 3H_2O$, gold chloride), tetraethyl orthosilicate (TEOS), ammonium hydroxide (NH_4OH), cysteamine, glycidyloxypropyl trimethoxysilane (GPTMS), ferricyanide, N-hydroxysuccinimide (NHS), and N-ethyl-N-(3-dimethylaminopropyl) carbodiimide (EDC) were obtained from Sigma-Aldrich, USA. Bovine serum albumin (BSA), anti-CA125 antibodies and CA125 antigens were from biomedical research lab, Singapore. All solutions used in experiments were prepared in milli-Q water.

Preparation of gold electrode

First of all, the gold electrode was prepared for construction of sandwich immunosensor. The glass wafer was sonicated in acetone, methanol for 45 min and then in deionized water. Then the piranha solution ($3H_2SO_4:1H_2O_2$) was used to clean the wafer at room temperature for 15 min. The wafer was again washed with deionized water and dried with nitrogen gas. A thin 100 nm film of gold was deposited by sputtering at a rate of 2 Å/s and pressure of 8.0×10^{-6} mbar, so that it can act as a working electrode in deposition process. Lastly, the gold electrode was again washed with deionized water and dried under the stream of nitrogen gas. Thereafter, the gold nanostructures were electrodeposited on these gold-coated glass wafers.

Electrodeposition of gold nanostructures

The electrodeposition of gold nanostructures (GNS) was performed in potentiostat mode. A three-electrode cell was used with gold as working electrode, Ag/AgCl as reference (CHI111, 3 M KCl) and platinum wire (CHI102, diameter 2.0 mm) as a counter electrode. All electrodepositions were

performed at room temperature. For deposition of GNS in step 2 as shown in Fig. 1, 0.1% of gold chloride in a 0.5 M HCl supporting electrolyte was used. The whole electro-deposition was executed at potentiostatic mode where the potential of working electrode is kept at − 1.0 V with respect to the Ag/AgCl reference electrode at pH = 4. The time of deposition was 40 min (Mahshid et al. 2016).

Synthesis of silicon nanoparticles

For synthesis of silicon nanoparticles (SiNPs), the sol–gel method was used (step A, shown in Fig. 1) (Wang et al. 2000). For SiNPs preparation, 1.5 mL of tetraethyl ortho-silicate (TEOS) was mixed in 1.7 mL of ammonium hydrox-ide, 1.0 mL of deionized water and 50 mL of ethanol in a round-bottom glass flask. This mixture was stirred at 40 °C for 3 h. 1.0 mL of TEOS was further added in the mixture and the reaction was continued for another 3 h. The solution was diluted ten times with deionized water and the ethanol was removed from the solution through rotary evaporator.

Immunosensor preparation

The electrodeposited GNS were used as a working elec-trode for sandwich immunosensor preparation as shown in Fig. 1. The electrode was cleaned in piranha solution and sonication was performed for 15 min in deionized water. The GNS-modified electrode was then incubated in 20 mM of cysteamine (10 μL) for 12 h at room temperature. The washing and drying were performed with phosphate buffer solution (PBS) in step 3 (functionalization). In step 4, a stock solution was prepared by mixing (i) 100 μL of 40 μg mL^{-1} anti-CA125 antibody solution with (ii) 100 μL of EDC–NHS (0.4 mg EDC and 1 mg NHS) solution for activation of –COOH group present in anti-CA125. These solutions were thoroughly mixed with shaker for 1 h (Zhong et al. 2015). A 5 μL of 20 μg mL^{-1} EDC–NHS activated anti-CA125 antibody from stock solution was dispersed on cysteamine-functionalized electrode and allowed to react overnight. The activated carboxyl group was then binded with the –NH$_2$ group of cysteamine leading to formation of amide bond. For removal of unbounded antibodies, the antibody-covered electrode was washed rigorously with PBS to remove unbounded antibodies. Then, 1% BSA was used to block the free binding sites for 30 min. The electrode was again washed with PBS three times and finally stored at 4 °C for further use in experiment.

Preparation of SiNPs–antibody complex

The surface of silicon nanoparticles were functionalized with epoxy groups by reacting with glycidyloxypropyl tri-methoxysilane (GPTMS) for protein immobilization in step B as shown in Fig. 1. The surface silanization reaction was carried out for 1 h with 5% GPTMS solution at room temper-ature. In step C, 7 μg mL^{-1} of anti-CA125 detector antibody

Fig. 1 Schematic of deposited gold nanostructures and different steps followed for the development of sandwich electrochemical immunosensor
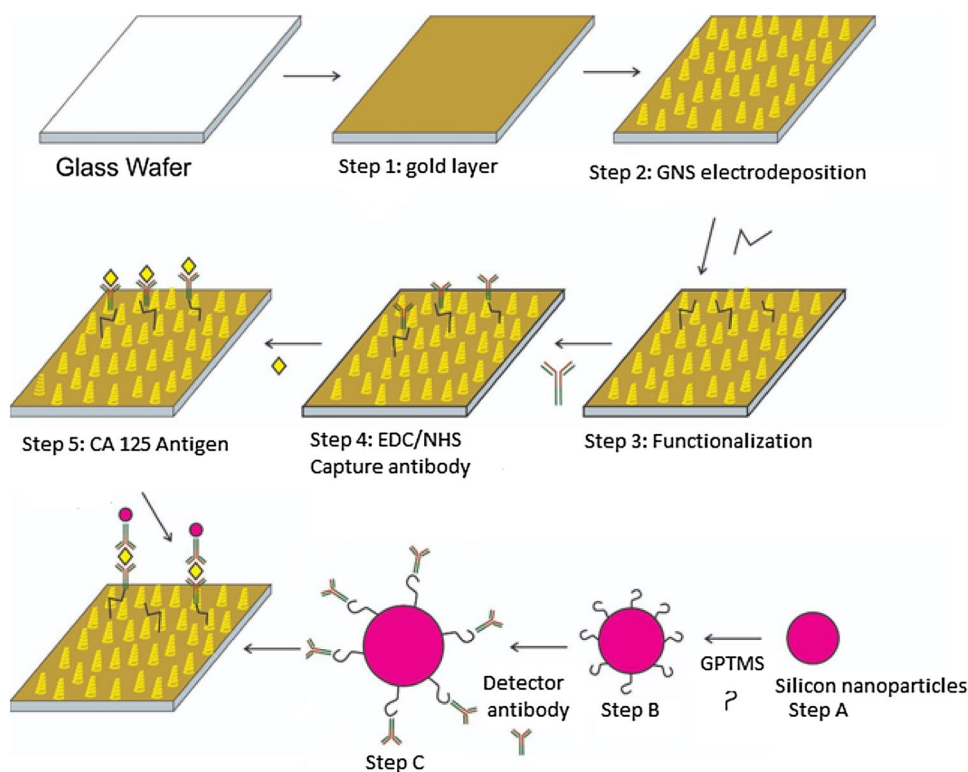
was added and allowed to incubate for 2 h at room temperature. The active sites were blocked using 1% BSA. Finally, for the removal of unbounded BSA the reaction mixture was centrifuged two times at 12,000 rpm for 15 min and particles were suspended in 0.01 M PBS solution.

Construction of CA 125 sandwich immunosensor

The Au/GNS/Ab-modified electrode was incubated with different concentrations of CA125 for 1 h at room temperature for antibody–antigen reaction in step 5 (Kumar et al. 2018). The electrode was rigorously washed to remove the loosely bound antigens. Finally, Au/GNS/Ab/CA125 electrode was incubated in SiNPs–Ab complex for 1 h at room temperature for sandwich formation. After extensive washing, electrochemical measurements were performed.

Characterization

Field emission scanning electron microscopy (FESEM) Hitachi Su8020, Japan was used to study the morphology of gold nanostructures and silica nanoparticles. The potential of SiNPs was measured using zeta potential apparatus (Malvern zetasizer nano ZSP), whereas the XRD spectra were recorded with Brooker model D8, wavelength 1.54 Å, voltage 40 kV and current 40 mA. The electrodeposition of GNS, electrochemical impedance, cyclic voltammetry and differential pulse voltammetry (DPV) were performed on CHI760D (CH Instruments, USA) electrochemical workstation. Electrochemical measurements were performed in 10 mL glass cell. The electrochemical data for differential pulse voltammetry were recorded from − 0.06 V to − 0.45 V with increment of 0.001 V vs. Ag/AgCl with a pulse amplitude of 50 mV. Cyclic voltammetry was performed between − 200 mV and 600 mV at 50 mV s^{-1} and used to assess the response of electrode. Electrodes were also characterized using electrochemical impedance spectroscopy (EIS). The EIS response was measured at frequencies between 100 kHz and 0.1 Hz and the impedance spectra were fitted to a Randles equivalent circuit to determine the charge transfer resistance. While, the Fourier transform infrared measurements were performed using model Nicolet 6700.

Results and discussion

Characterization of GNS

The gold nanostructures (GNS) were electrodeposited on a gold electrode at pH = 4 for 40 min. Field emission scanning electron microscopy (FESEM) was performed to study the surface morphology of GNS and the images of the structures obtained are shown in Fig. 2a, b. It can be observed from Fig. 2a (low-magnification image) and Fig. 2b (high-magnification image) that hierarchical GNS were formed and these nanostructures compactly occupied the whole electrode surface. It can be observed in Fig. 2b that the aggregates of nanocrystals started to grow with a larger size, suggesting the slow growth of nuclei formation on substrate. Due to the decrease in growth rate, further growth of gold occurred on already formed gold nuclei. Therefore, some hierarchical GNS were formed due to a decrease in reduction rate of gold chloride at pH 4.

Figure 2c represents the XRD spectra obtained for GNS. The observed diffraction peaks were (111), (200), (220), (311) and (222). These peaks demonstrate that the electrodeposited GNS were purely composed of crystalline face centered cubic (FCC) structure (Tian et al. 2006). The chemical composition of GNS was characterized by EDX as shown in Fig. 2d. It indicates that the prepared gold electrode having electrodeposited GNS was purely composed of gold as only gold peaks were observed. Therefore, there was no impurity detected in the GNS electrode.

Characterization of SiNPs

The size and surface morphology of bare and functionalized silicon nanoparticles (SiNPs) were studied using FESEM and the images obtained are shown in Fig. 3a, b, c. Figure 3a represents the bare SiNPs, it can be observed that spherical sized silicon nanoparticles were obtained with an average diameter of 87.9 ± 3.2 nm. The bare SiNPs represents fizzy boundaries with some agglomeration. This was due to the high surface energy possessed by the SiNPs (Yina et al. 2017). With modification of SiNPs with GPTMS (Fig. 3b), the particles showed clear boundaries and reduced agglomeration. However, again the agglomeration effect was observed when SiNPs were modified with detection antibody. The average size of the SiNPs increased to 113.6 ± 5.3 nm and their surface became rough compared to bare SiNPs as can be seen in FESEM image (Fig. 3c). This suggested that the surface of SiNPs was modified with target antibody.

The zeta potential measurements were performed to examine the formulation stability of SiNPs. The zeta potential refers to the electrostatic potential between surface of nanoparticles and the solvent. It is very sensitive to the chemical groups present on the surface of solid materials. The zeta potential of SiNPs was measured at different steps of modification. The value of zeta potential came out to be − 27.5 mV in pure water (pH 6.8) as shown in Fig. 3d. The negative sign was due to the presence of hydroxyl group on the surface of silicon nanoparticles (Rafique et al. 2014). After epoxy group modification, this potential shifted towards positive value of + 15.2 mV, indicating the replacement of hydroxyl group with epoxy (Kardys et al. 2013). With further modification with anti-CA125 antibody, the
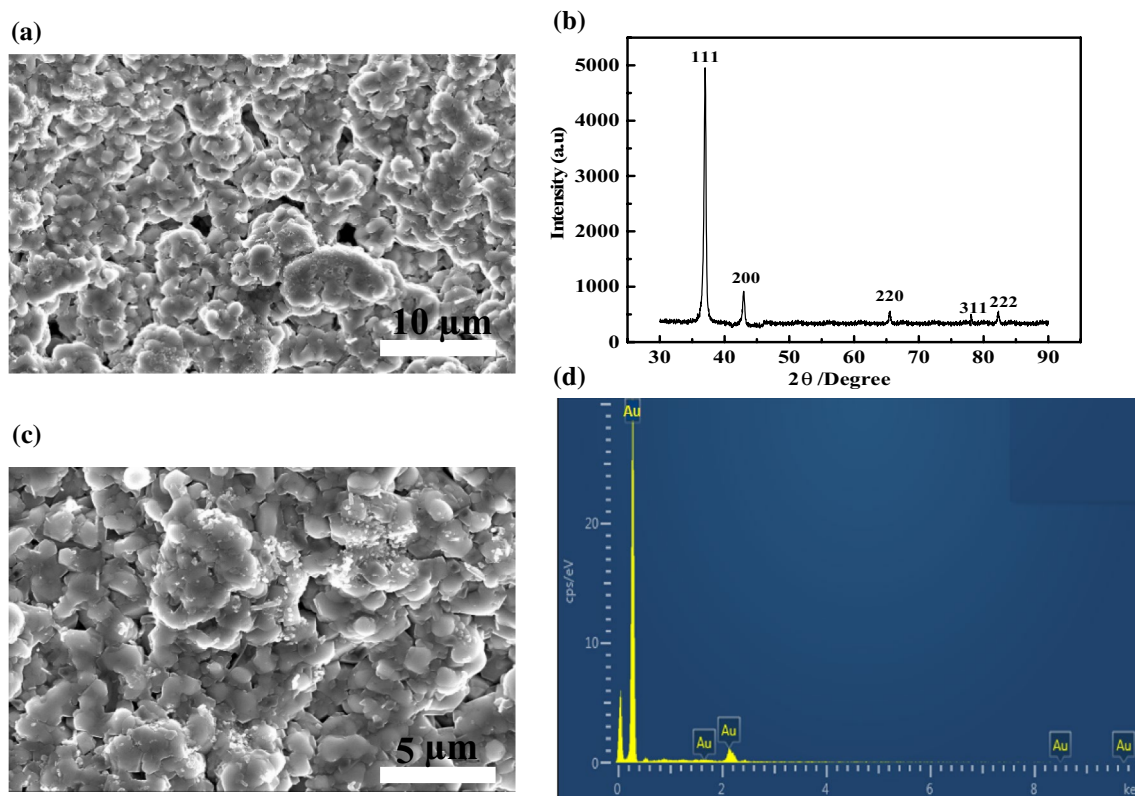
Fig. 2 Characterization of gold nanostructures electrodeposited on gold electrode (**a**, **b**) surface morphology of gold nanostructures by field emission scanning electron microscopy (**c**) X-ray diffraction and (**d**) energy-dispersive X-ray spectroscopy analysis (EDX)

potential again shifted towards negative value of -25.8 mV as shown in Fig. 3f. This shift in potential demonstrated that the silicon nanoparticles were modified with anti-CA125 target antibody.

The FTIR analysis was performed to study the chemical structure of bare and functionalized SiNPs as shown in Fig. 4. Figure 4 showed a broad peak at about 3447 cm^{-1}. This peak was due to the stretching vibration of –OH on the surface of SiNPs. In Fig. 4 the peak at 1447 cm^{-1} was due to the C–H stretching bands. The characteristics peaks at 1150 cm^{-1} and 840 cm^{-1} dominate the spectra of silicon nanoparticles samples. This was mainly due to stretching and bending vibration of silicon and oxygen (Gholami et al. 2013). The asymmetric vibration of O–Si–O was indicated by the peak at 1150 cm^{-1}. While, the peak at 840 cm^{-1} can be ascribed to symmetric stretching vibration of O–Si–O. These peak confirmed that SiNPs were obtained via the Stober method. The SiNPs modified with GPTMS are shown by a red line in Fig. 4. A new peak around 950 cm^{-1} appeared due to epoxy group of GPTMS (Schramm et al. 2004). The decrease and shift in absorption peak was observed at 3447 cm^{-1} due to –OH stretching vibration (Qin et al. 2009). It was attributed to the fact that –OH groups on SiNPs surface were substituted by epoxy group of GPTMS.

It suggested that epoxy group has been introduced on the surface of SiNPs.

Figure 4 shows the FTIR spectrum of SiNPs-Ab; the bands at 980 cm^{-1}, 1100 cm^{-1} and 1250 cm^{-1} are the main characteristic peaks of Si–O–Si bonds vibrational modes, which recognizes the O–Si–O vibrational band, Si–O bending vibrational band, and Si–O–Si stretching vibration band, respectively (Chitra and Annadurai 2013). While the strong peak observed near 3300 cm^{-1} resulting from assymetric stretching vibrations of the –CH2 groups confirmed the presence of amine groups of anti-CA125.

Experimental conditions

The concentration of solution used for capture and detection antibody greatly affects the performance of immunosensor. Therefore, the concentration of solution for capture and detection antibody was optimized. For this purpose, three different concentrations of capture and detection anti-CA125 were used and their effect on blank solution was evaluated as shown in Fig. 5a. The concentration used was 10, 20 and 30 µg mL^{-1} for capture anti-CA125 antibody and 5, 7 and 10 µg mL^{-1} for detection anti-CA125 antibody, respectively.
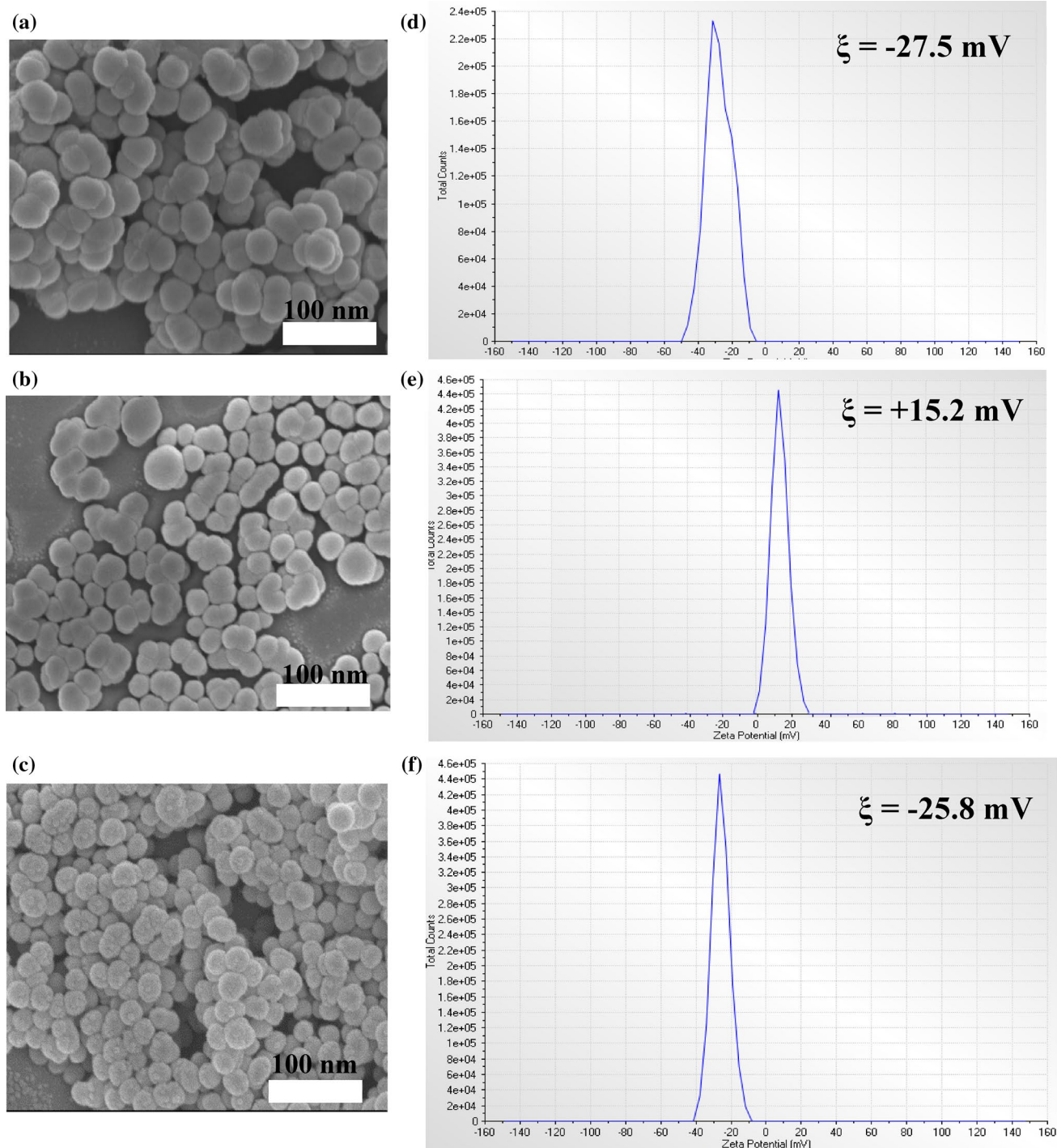
Fig. 3 FESEM and zeta potential measurements of (**a**) bare silicon nanoparticle (**b**) silicon nanoparticles modified with GPTMS (**c**) attachment of detection anti-CA125 on silicon nanoparticle surface. **d–f** represents the zeta potential measurements of different modifications of silicon nanoparticles

It was observed that the blank solution signal decreased with increase in concentration of capture anti-CA125 antibody at fixed concentration of 5 and 7 μg mL^{-1} for detection of anti-CA125 antibody. This suggested that a high concentration of capture anti-CA125 antibody formed complete, compact and regular functionalization on gold nanostructured electrode which prevented non-specific adsorption of detection anti-CA125 antibody. While, an opposite trend was observed in blank solution signal when capture anti-CA125 antibody was fixed to 20 and 30 μg mL^{-1}. The high
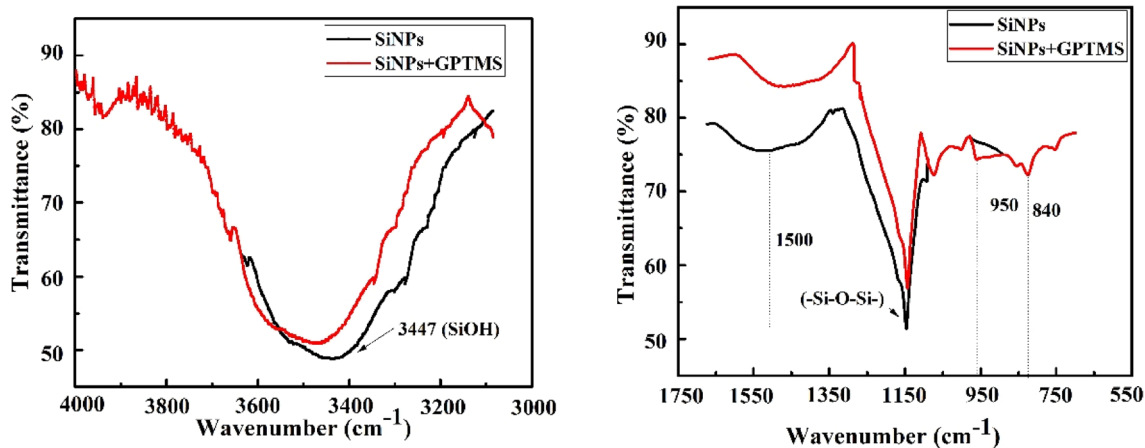
Fig. 4 FTIR spectra of bare silicon nanoparticle (black line) and modified with 1% GPTMS (redline). The scale of wavenumber of graph is from 4000 to 3000 cm^{-1} (left) and from 1750 to 550 cm^{-1} (right), respectively
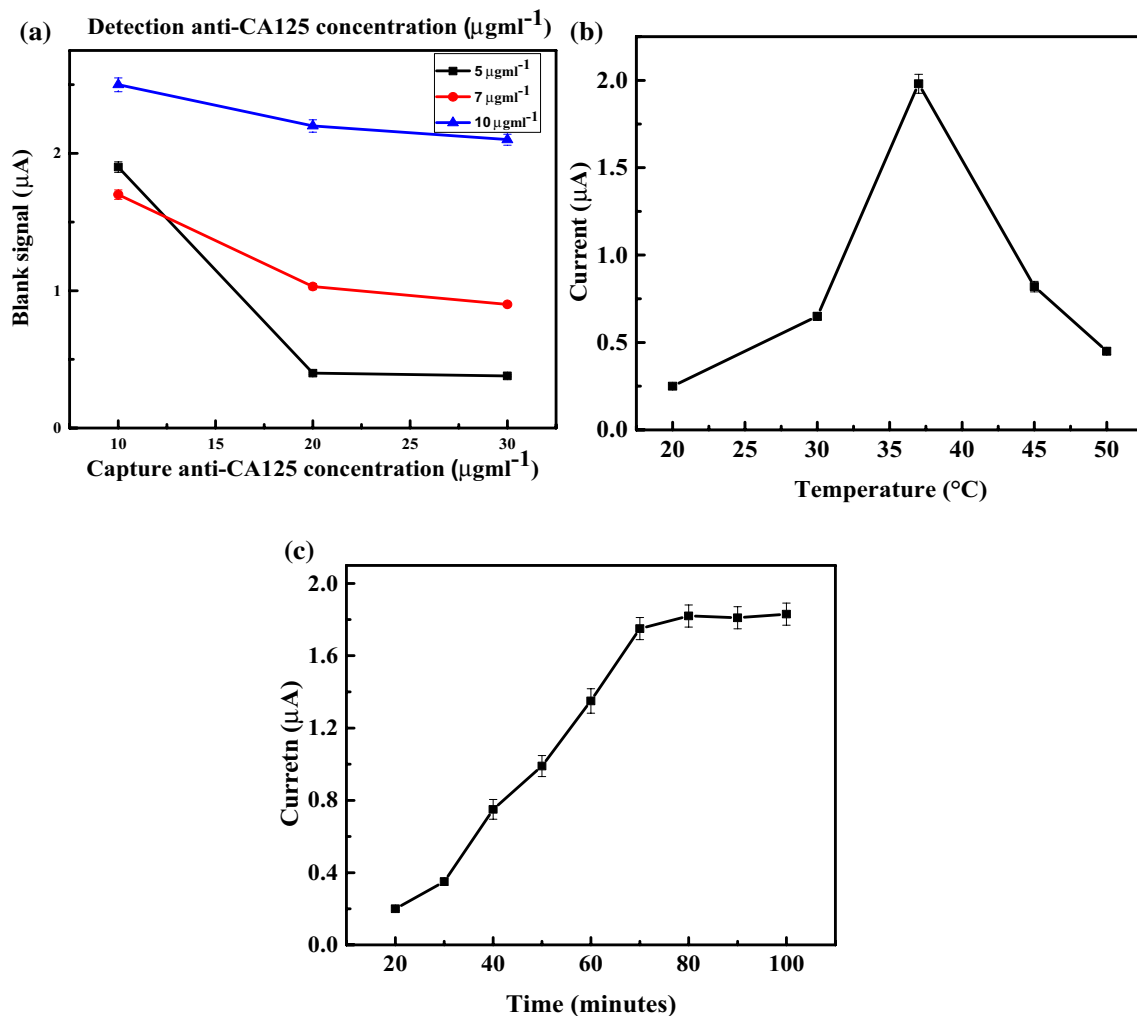

Fig. 5 Effect on the response peak current for different concentrations of **a** capture and detectionanti-CA 125 antibody (complex formation of antibody—antigen) **b** variation of current as a function of temperature **c** current variation with the time of incubation

concentration of detection anti-CA125 antibody could promote its non-specific binding. It can be seen that with 10 μg mL^{-1} of anti-CA125 capture antibody, the signal did not decreased significantly even the concentration of detection anti-CA125 antibody was reduced to 7 μg mL^{-1}. Consequently, the concentration of capture and detection anti-CA125 antibody was fixed to 20 μg mL^{-1} and 7 μg mL^{-1}, respectively.

Afterwards, the effect of incubation time and temperature was optimized for antibody–antigen complex formation. Cyclic measurements were performed and change in the current was observed for this purpose. The plot of current obtained as a function of incubation time and temperature is shown in Fig. 5b, c. Figure 5b indicates that the maximum immunosensor response was obtained at 37 °C, so this temperature was selected for antibody–antigen reaction. However, the current increased with incubation time and got saturated at about 80 min. So, optimally 60 min incubation time was chosen for sandwich immunosensor of CA125 antigen.

The acidic or basic medium can affect the biocatalytic performance of immunosensor. Therefore, the effect of pH on immunosensor performance was investigated by performing electrochemical measurements in the range from acidic to basic medium. The concentration of capture and detection anti-CA125 antibody was fixed to 20 μg mL^{-1} and 7 μg mL^{-1}. Figure 5 summarizes the current response obtained at different pH values. The maximum current was obtained at pH = 7, this value was taken as optimized value for all the experiments to obtain better biochemical activity.

Construction of sandwich immunosensor

The cyclic voltammetry (CV) measurements were performed in 5 mM [Fe(CN)$_6$]$^{3-/4-}$ mixed in 0.1 M KCl solution from − 0.2 V to 0.6 V. The CV obtained at each step of preparation of immunosensor is shown in Fig. 6a, b. Figure 6a shows the CV of plane gold electrode and Fig. 6b for GNS electrode at different steps of preparation of sandwich immunosensor. It can be seen that well-defined redox peaks of 5 mM [Fe(CN)$_6$]$^{3-/4-}$ were observed at the electrode surface with average current of 98 μA for plane gold electrode. A significant increase in current was observed from 96 μA to 128 μA after electrodeposition of gold nanostructures on gold electrode showing improved redox behavior on gold nanostructured electrode as shown in Fig. 6b. The large surface area (Ramulu et al. 2013) and roughness (Sanzó et al. 2016) provided by the deposited GNS contributed the enhancement in current. This suggests that the GNS electrode may acquire a high amount of capturing molecules compared to plane Au electrode. So, GNS-modified electrode can exhibit high sensitivity towards detection of CA125 antigen.

With the immobilization of cysteamine, the current decreased from 102 to 93 μA for plane Au electrode. While, a prominent decrease in current from 128 to 86 μA was observed in case of GNS-modified electrode. With further immobilization of capture anti-CA125 antibody the current further reduced to 89 μA and 61 μA for plane Au and GNS electrode, respectively. This may be due to the induction of effective barrier layer by immobilization of antibody (Zhu et al. 2015). Furthermore, when CA125 antigen immobilization occurred on electrode, a decrease in current from 89 to 73 μA and 61 to 55 μA was observed for plane and GNS electrode, respectively. This shows successful immobilization of CA125 antigen on electrode. Again, a prominent decrease in current was observed from 55 to 35 μA with immobilization of detection anti-CA125 antibody. This again demonstrates that the effective barrier layer was introduced which reduced the diffusion of redox probe towards electrode surface which results in the decrease of current value. Another important observation from CV measurement demonstrated that the prominent decrease in current was observed in GNS electrode compared to plane Au electrode which suggests that GNS-modified electrode was a favorable surface for CA125 antigen detection. This suggests that the synthesized sandwich immunosensor shows enhanced response by deposition of GNS.

Further, electrochemical impedance measurements were performed to study the electron transfer kinetics behavior on plane Au electrode and GNS electrode at different steps of preparation of immunosensor as shown in Fig. 6c, d. Figure 6c represents the Nyquist plot of (i) Au electrode (ii) Au/capture anti-CA125 antibody, (iii) Au/anti–CA125 antibody/antigen and (iv) GNS/capture anti–CA125 antibody/antigen/detection anti–CA125 antibody electrode in 5 mM [Fe(CN)$_6$]$^{3-/4-}$ mixed in 0.1 M KCl solution in frequency range from 10 μHz to 20 kHz. The impedance spectrum consists of a straight line in low-frequency region which represents the diffusion controlled process and a semicircle in high-frequency region representing charge transfer resistance (Kaushik et al. 2018). The impedance spectrum can be analyzed by use of Randle equivalent circuit as shown in inset of Fig. 5c in which R_u is the solution resistance, R_P (the charge transfer resistance), W_d (Warburg impedance), and CPE was constant phase element (Li et al. 2017). An important parameter R_P in Nyquist plot was evaluated by fitting the spectra with equivalent circuit. The value of R_P came out to be 1200 Ω for plane Au electrode (Fig. 5c). This value further increased to 1500 Ω, 1900 Ω and 2200 Ω after attachment of capture antibody, CA125 antigen and SiNPs conjugated with target antibody, respectively.

While, in case of GNS electrode the value of charge transfer resistance decreased to 500 Ω after electrodeposition of GNS (curve ii, Fig. 6d). This was due to the large surface area provided by the gold nanostructures.
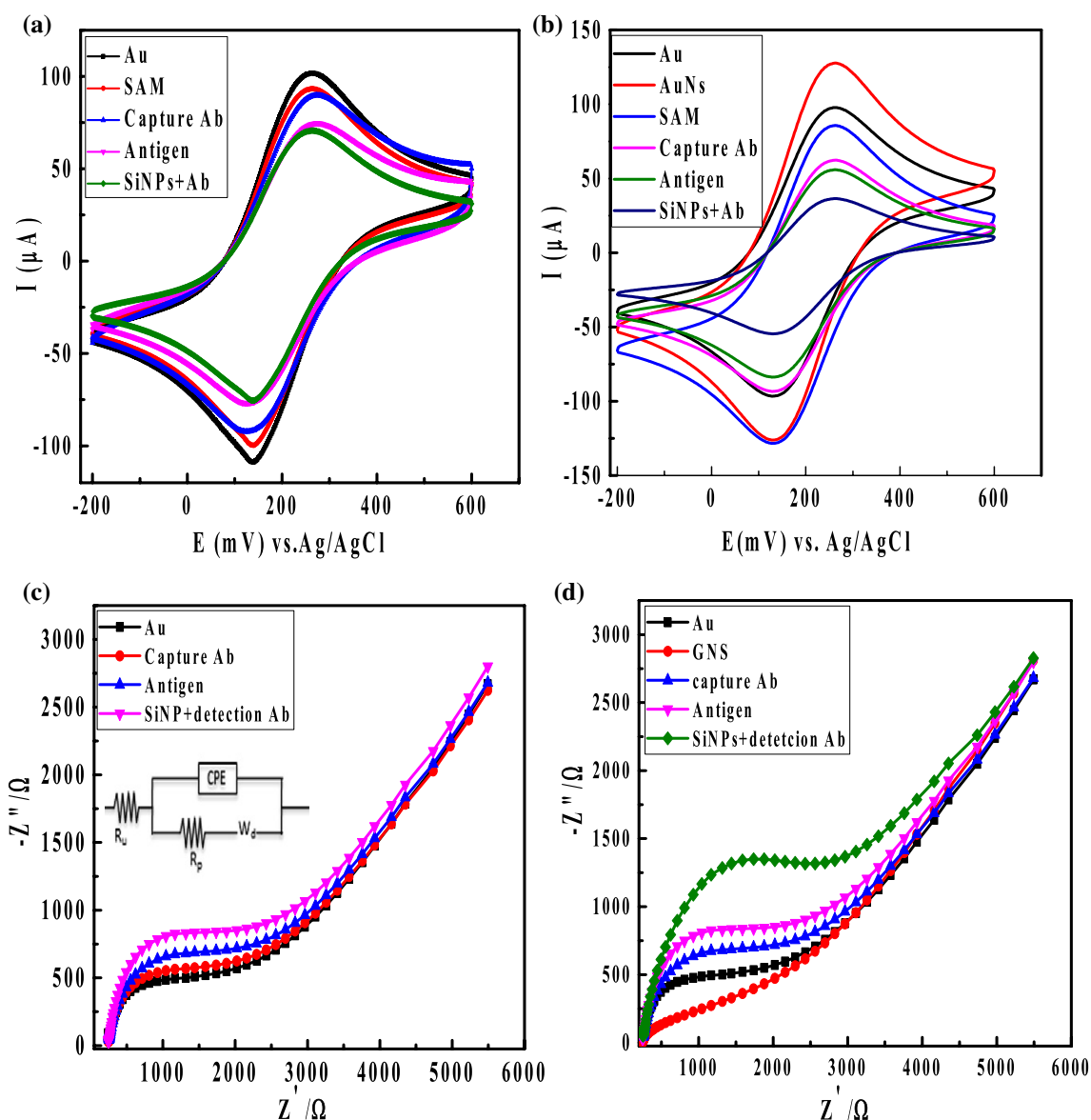
Fig. 6 Effect of electrochemical response of sandwich immunosensor at different steps of preparation. The cyclic voltammetry of **a** plane gold electrode **b** gold nanostructured electrode, Nyquist plot for **c** plane gold electrode and **d** gold nanostructured electrode in 5 mM $[Fe(CN)_6]^{3-/4-}$ mixed in 0.1 M KCl

The immobilization of capture anti-CA125 antibody through cysteamine on GNS electrode formed a blocking layer which reduced the current on electrode surface and increased the resistance value to 2100 Ω. Further increase in R_P to 2500 Ω, and 3100 Ω was observed after binding of CA125 antigen and detection of anti-CA125 antibody. This suggest that at every step of immunosensor preparation an additional barrier layer was added which reduced the current and increased the resistance. These results were in agreement with the CV measurements. Therefore, GNS electrode was investigated against different concentrations of CA125 antigen.

Electrochemical detection of CA 125

The response of GNS/anti-CA125 antibody/CA125 antigen/SiNPs was studied in the concentration range from 1 fg mL^{-1} to 1 µg mL^{-1} using differential pulse voltammetry (DPV). The DPV curves obtained in this concentration range are shown in Fig. 7a(i–xi). The maximum value of average current (I_p) obtained for anti-CA125 capture antibody was 9.75 µA. This value of current was reduced to 9.26 µA after attachment of CA125 antigen for 1 fg mL^{-1}. This current was further reduced to 6.5 µA when the concentration of CA125 antigen was 1 ng mL^{-1}. This demonstrates
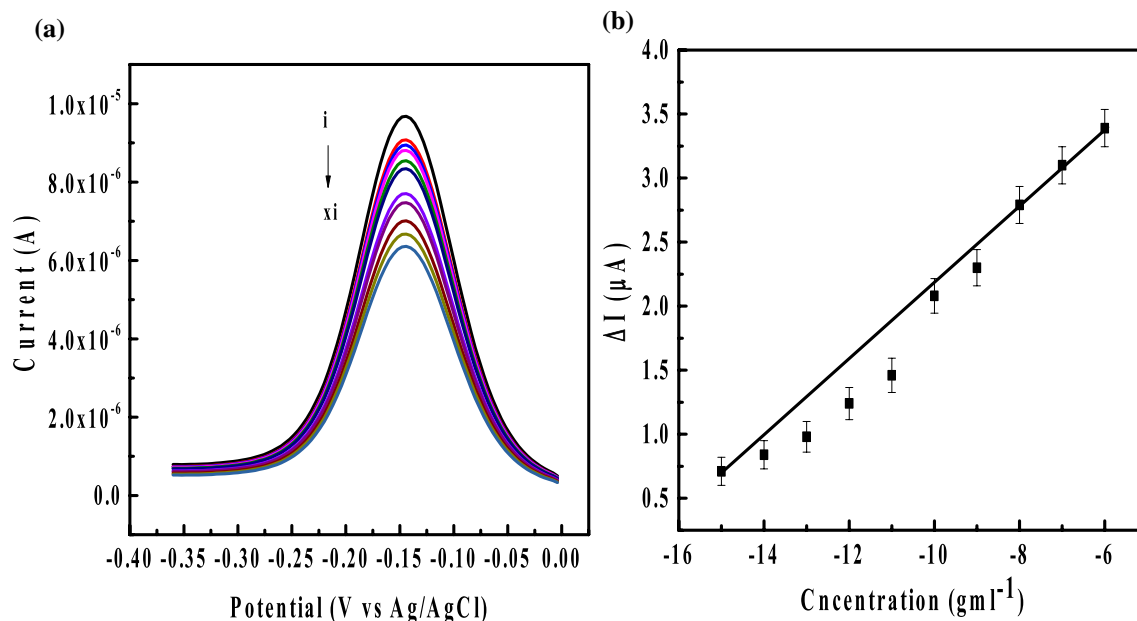
(a)

(b)

Fig. 7 **a** Differential pulse voltammetry response for different concentrations of CA125 antigen ranges from (i) anti-CA125 antibody (ii) 10^{-15} (iii) 10^{-14} (iv) 10^{-13} (v) 10^{-12} (vi) 10^{-11} (vii) 10^{-10} (viii) 10^{-9} (ix) 10^{-8} (x) 10^{-7} (xi) 10^{-6} **b** calibration plot of DPV peak current versus CA125 antigen concentration under optimal condition

that complex formation of antibody–antigen on electrode surface reduced the charge transfer process which reduced the current (Ma et al. 2016). It can be deduced from here that the I_p (maximum peak current) values were inversely related to the concentration of CA125 antigen. Further, the calibration curve was plotted between the change in current ($\Delta I = I_{ab} - I_{ag}$, where I_{ab} is the current obtained after anti-CA 125 antibody and I_{ag} the current obtained after CA125 antigen) as a function of concentration as shown in Fig. 7b. A linear relation was observed between ΔI and CA125 antigen concentration obeying the following equation:

$$\Delta I = 0.3199 \, (\text{concentration g mL}^{-1}) + 5.11$$

The regression coefficient by linear fit came out to be 0.9872. From here, the theoretical value of limit of detection (LOD) was calculated using the formula LOD $= 3 \times$ S.D/sensitivity, where sensitivity was obtained from linear fit and S.D was the standard deviation of the blank solution. The theoretical value of LOD came out to be 0.05 fg mL^{-1}. This showed that the proposed GNS modified electrode is a simple approach to detect CA125 antigen up to 0.05 fg mL^{-1} with a wide dynamic range of 1 fg mL^{-1} to 1 μg mL^{-1}. This low LOD was obtained due to enhanced surface area provided by deposited GNS which increased the loading capacity of anti-CA125 capture antibody on immunosensor surface. The improvement in LOD would be quite useful for primal detection of ovarian cancer. The presence of

malignancy in patients with a pelvic mass is predicted by the tumor marker CA125. In advanced cancer, the elevated (> 35 U mL^{-1}) value of CA125 is observed in 80% cases. While, in early stages fewer values were observed in 50% of cases (Gazze et al. 2018). The threshold value for CA125 is 35 U mL^{-1}. The three-dimensional GNS electrode showed drastic improved LOD, which could be useful for the clinical diagnosis for early detection of CA125 level for ovarian cancer.

To further explore the worth of prepared sandwich electrochemical immunosensor, the sensitivity and dynamic range of the immunosensor were compared with other reported electrochemical immunosensors (Guo et al. 2013; Huang et al. 2017; Ravalli et al. 2013; Quintero-Jaime et al. 2019) as shown in Table 1. Table 1 shows that the sensitivity and dynamic range of the GNS sandwich electrochemical immunosensor is better than the reported work. Besides, the prepared electrodeposited 3D-GNS electrode is simple, cost-effective and greener than the other nanocomposites.

Stability and reproducibility of immunosensor

The reproducibility of sandwich electrochemical immunosensor was examined by computing intra-assay and inter-assay coefficient of variation. For intra-assay variation coefficient, the measurement of prepared immunosensor was repeated five times at CA125 antigen concentration of 1 ng mL^{-1}. While, the inter-assay variation coefficient was determined by measuring five different immunosensor under

Table 1 Comparison table for different types of immunosensor

Electrode modification	Biomarkers	Concentration range	LOD	References
Graphene with PANI film	CA125	0.96 pg–15.2 ng μL^{-1}	0.923 ng μL^{-1}	Gazze et al. (2018)
Au@Pd core–shell nanocomposites	CA125	0.002–20 U mL^{-1}	0.001 U mL^{-1}	Guo et al. (2013)
Polythionine–Au composites	Carbohydrated antigens (CA 19-9)	6.5–520 U mL^{-1}	0.26 U mL^{-1}	Huang et al. (2017)
Gold nanoparticles-modified screen-printed graphite electrode	CA125	0–100 U mL^{-1}	6.7 mL^{-1}	Ravalli et al. (2013)
Carbon nanotube-modified Au electrode	PSA	0–6 mg mL^{-1}	1 ng mL^{-1}	Quintero-Jaime et al. (2019)
Three-dimensional nanostructured electrode	CA125	1 fg–1 μg mL^{-1}	0.05 fg mL^{-1}	Present work

Table 2 Inter-assay variation results for prepared immunosensor

Immunosensor	Mean response (μA)	Standard deviation	CV (%)
$n = 5$	2.246	0.1016	4.52
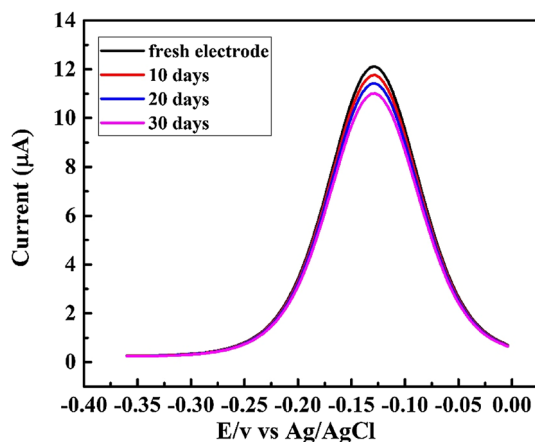
Fig. 8 Differential pulse voltagram response of sandwich gold nanostructured-modified immunosensor with respect to the storage days

buffer solution. The DPV measurements were performed after every 5 days on the same immunosensor. The DPV curves obtained are shown in Fig. 8. It can be seen that the current values were 98.2%, 95.5% and 92.1% of its initial values after 10, 20 and 30 days, respectively, showing good stability of the prepared immunosensor.

Application of immunosensor for human CA 125 levels

The prepared sandwich immunosensor was cross-examined with specific CA125 antigen biomarker which is labeled as control sample and with three different human samples. The clinical samples were measured five times ($n = 5$) to obtain the precision. Table 3 shows the average levels of CA125 obtained from prepared electrode in different human serum samples. The lowest level detected with the prepared immunosensor using control sample was 1 fg mL^{-1}. Serum samples were spiked with CA125 at concentrations of 1, 10 and 1 pg mL^{-1}, which were tested using the immunosensor. The average level detected in human serum was 1.80 pg mL^{-1}, 10.52 pg mL^{-1} and

Table 3 Comparison of developed immunosensor for CA125 biomarker and different human serum samples

Sample no	CA125 biomarker	Serum contained with CA125 (pg mL^{-1})	CA125 added into human serum (pg mL^{-1})	Average CA125 detected ($n = 5$)	RSD (%)	R (%)
1	1 fg mL^{-1}	0	1	1.80	1.2	108
2	1 fg mL^{-1}	0	10	10.52	2	105
3	1 fg mL^{-1}	0	1	1.13	3.9	113

same experimental conditions. The results, summarized in Table 2, show inter-assay variation between the immunosensor with CV% < 15%. So, it can be attributed that the prepared immunosensor showed good reproducibility.

The shelf life of electrochemical immunosensor was examined by keeping the electrode at 4 °C in phosphate

1.13 pg mL^{-1} in sample 1, 2 and 3, respectively. The calculated relative standard (RSD) is shown in Table 3. The recovery value ranged from 108 to 113%. This result showed that developed immunosensor has potential applications for detection of CA125 levels in clinical samples.

Conclusion

In this work, a simple one-step electrodeposition method was employed to develop a sandwich electrochemical immunosensor. Due to high conductivity and surface area provided by the electrodeposited gold nanostructures, the prepared immunosensor showed excellent sensitivity and specificity towards detection of CA125 antigens detection. The prepared immunosensor was sandwiched using silicon nanoparticles conjugated secondary antibody which increases the fixation capacity of silicon nanoparticles on CA125 antigens. Furthermore, the gold nanostructures improves the electron transfer ability of immunosensor. The developed sandwich immunosensor showed limit of detection of 0.05 fg mL^{-1} with wide dynamic range from 1 fg mL^{-1} to 1 µg mL^{-1}. The immunosensor also demonstrated good sensitivity to three different human serum samples. This indicates that the proposed method has clinical applications in the diagnosis and monitoring of cancer at different stages.

Compliance with ethical standards

Conflict of interest The authors declare no conflicts of interest.

References

Alizadeh L, Zarebkohan A, Salehi R, Ajjoolabady A, Yamchi AR (2019) Chitosan-Based Nanotherapeutics for Ovarian Cancer Treatment. J Drug Target 27:239–852. https://doi.org/10.1080/1061186X.2018.1564923

Bray F, Ferlay J, Soerjomataram I, Siegel RL, Torre LA, Jemal A (2018) Global cancer statistics 2018: GLOBOCAN estimates of incidence and mortality worldwide for 36 cancers in 185 countries. CA Cancer J Clin 68:394–424. https://doi.org/10.3322/caac.21492

Cheng L, Yang L, Meng F, Zhong Z (2018) Protein nanotherapeutics as an emerging modality for cancer therapy. Adv Healthc Mater 7:1800685–1800694. https://doi.org/10.1002/adhm.201800685

Chitra K, Annadurai G (2013) Fluorescent silica nanoparticles in the detection and control of the growth of pathogen. J Nanotechnol 2013:1–7. https://doi.org/10.1155/2013/509628

Dochez V, Caillon H, Vaucel E, Dimet J, Winer N (2019) Biomarkers and algorithms for diagnosis of ovarian cancer: CA125, HE4, RMI and ROMA, a review. J Ovarian Res 12:28–37. https://doi.org/10.1186/s13048-019-0503-7

Gazze A, Ademefun R, Conlan RS, Teixeira SR (2018) Electrochemical impedance spectroscopy enabled CA125 detection; toward early ovarian cancer diagnosis using graphene biosensors. J Interdiscip Nanomed 3:82–88. https://doi.org/10.1002/jin2.40

Gholami MA, Hahne H, Wu Z, Auer FJ, Meng C, Wilhelm M, Kuster B (2013) Global proteome analysis of the NCI-60 cell line panel. Cell Rep 4:609–620 https://doi.org/10.1016/j.celrep.2013.07.018

Guo A, Wu D, Ma H, Zhang Y, Li H, Du B, Wei Q (2013) An ultrasensitive enzyme-free electrochemical immunosensor for CA125 using Au@Pd core–shell nanoparticles as labels and platforms for signal amplification. J Mater Chem B 1:4052–4059. https://doi.org/10.1039/C3TB20574F

Huang Z, Jiang Z, Zhao C, Han W, Lin L, Liu A, Weng S, Lin X (2017) Simple and effective label-free electrochemical immuno-assay for carbohydrate antigen 19–9 based on polythionine-Au composites as enhanced sensing signals for detecting different clinical samples. Int. J. Nanomedicine 12: 3049–3058 https://doi.org/10.2147/IJN.S131805. https://www.cancerresearchuk.org/health-professional/cancer-statistics/statistics-by-cancer-type/ovarian-cancer

Jeyaraj M, Sathishkumar GS, MubarakAli D, Rajesh M, Arun R, Kapildev G, Manickavasagam M, Thajuddin N, Premkumar K, Ganapathi A (2013a) Biogenic silver nanoparticles for cancer treatment: an experimental report. Colloids Surf B 106:86–92. https://doi.org/10.1016/j.colsurfb.2013.01.027

Jeyaraj M, Rajesha M, Arunb R, MubarakAli D, Sathishkumar G, Sivanandhana G, Deva GK, Manickavasagama M, Premkumar K, Thajuddinc N, Ganapathi A (2013b) An investigation on the cytotoxicity and caspase-mediated apoptotic effect of biologically synthesized silver nanoparticles using Podophyllum hexandrum on human cervical carcinoma cells. Colloids Surf B 102:708–717. https://doi.org/10.1016/j.colsurfb.2012.09.042

Jeyaraj M, Arun R, Sathishkumar G, Davoodbasha M, Rajesh M, Ganeshan S, Gnanajothi K, Manickavasagam M, Nooruddin T, Ganapathi A (2014) An evidence on G2/M arrest, DNA damage and caspase mediated apoptotic effect of biosynthesized gold nanoparticles on human cervical carcinoma cells (HeLa). Mater Res Bull 52:15–24. https://doi.org/10.1016/j.materresbull.2013.12.060

Kardys AY, Bharali DJ, Mousa SA (2013) Amino-functionalized silica nanoparticles. In vitro evaluation for targeted delivery and therapy of pancreatic cancer. J Nanotechnol 768724:1–8. https://doi.org/10.1155/2013/768724

Kaushik A, Yndart A, Kumar S, Jayant RD, Vashist A, Brown AN, Li CZ, Nair M (2018) A sensitive electrochemical immunosensor for label-free detection of Zika-virus protein. Sci Rep 8:9700–9705. https://doi.org/10.1038/s41598-018-28035-3

Kim JY, Cho CH, Song HS (2017) Targeted therapy of ovarian cancer including immune check point inhibitor. Korean J Intern Med 32:798–804. https://doi.org/10.3904/kjim.2017.008

Kumar N, Sharma S, Nara S (2018) Dual gold nanostructure-based electrochemical immunosensor for CA125 detection. Appl Nanosci 8:1843–1853. https://doi.org/10.1007/s13204-018-0857-y

Li H, Ye H, Li A, Wang X, Hou P, Wang C, Chen K, Zhao C (2017) A highly sensitive electrochemical impedance immunosensor for indole-3-acetic acid and its determination in sunflowers under salt stress. RSC Adv 7:54416–54421. https://doi.org/10.1039/c7ra09979g

Lorenzo DG, Ricci G, Severini GM, Romano F, Biffi S (2018) Imaging and therapy of ovarian cancer: clinical application of nanoparticles and future perspectives. Theranostics 8:4279–4294. https://doi.org/10.7150/thno.26345

Ma H, Sun J, Zhang Y, Bian C, Xia S, Zhen T (2016) Label-free immunosensor based on one-step electrodeposition of chitosan-gold nanoparticles biocompatible film on Au microelectrode for determination of aflatoxin B1 in maize. Biosen Bioelectron 80:222–229. https://doi.org/10.1016/j.bios.2016.01.063

Mahshid S, Adam HM, Mahshid SS, Burgess IB, Safaei TS, Sargent EH, Kelley SO (2016) Mechanistic control of the growth

of three-dimensional gold sensors. J Phys Chem C 120:21123–21132. https://doi.org/10.1021/acs.jpcc.6b05158

Mehnath S, Arjama M, Rajan M, Arokia VM, Murugaraj J (2018) Polyorganophosphazene stabilized gold nanoparticles for intracellular drug delivery in breast carcinoma cells. Process Biochem 72:152–161. https://doi.org/10.1016/j.procbio.2018.06.006

Menon U, Gentry MA, Hallett R, Ryan A, Burnell M, Sharma A, Lewis S, Davies S, Philpott S, Lopes A, Godfrey K, Oram D, Herod J, Williamson K, Seif MW, Scott I, Mould T, Woolas R, Murdoch J, Dobbs S, Amso NN, Leeson S, Cruickshank D, Mcguire A, Campbell S, Fallowfield L, Singh N, Dawnay A, Skates SJ, Parmar M, Jacobs I (2009) Sensitivity and specificity of multimodal and ultrasound screening for ovarian cancer, and stage distribution of detected cancers: results of the prevalence screen of the UK Collaborative Trial of Ovarian Cancer Screening (UKCTOCS). Lancet Oncol 10:327–340. https://doi.org/10.1016/S1470-2045(09)70026-9

Orr B, Edwards RP (2018) Diagnosis and treatment of ovarian cancer. Hematol Oncol Clin North Am 32:943–964. https://doi.org/10.1016/j.hoc.2018.07.010

Paris JL, María VR (2018) Nanostructures for imaging, medical diagnostics and therapy. Fundamentals of nanoparticles, Elsevier, pp 1–28. https://www.sciencedirect.com/science/article/pii/B9780323512558000001X.

PDQ Adult Treatment Editorial Board, PDQ Cancer Information Summaries Ovarian (2019) Epithelial, Fallopian Tube, and Primary Peritoneal Cancer Treatment (PDQ®): Patient Version. National Cancer Institute (US). https://www.ncbi.nlm.nih.gov/pubmed/26389163.

Qin Z, Rong H, Hong GL (2009) One-step and high-density protein immobilization on epoxysilane-modified silica nanoparticles. Chin Sci Bull 54:2620–2626. https://doi.org/10.1007/s11434-009-0210-7

Quintero-Jaime AF, Murcia AB, Diego Amorós C, Morallón E (2019) Nanotubes modified with au for electrochemical detection of prostate specific antigen: effect of au nanoparticle size distribution. Front Chem 7:147–159. https://doi.org/10.3389/fchem.2019.00147

Rafique S, Bin W, Bhatti AS (2014) Electrochemical immunosensor for prostate-specific antigens using a label-free second antibody based on silica nanoparticles and polymer brush. Bioelectrochemistry 101:75–83. https://doi.org/10.1016/j.bioelechem.2014.08.001

Ramulu TS, Venu R, Sinha B, Lim B, Jeon SJ, Yoon SS, Kim CG (2013) Nanowires array modified electrode for enhanced electrochemical detection of nucleic acid. Biosen Bioelectron 40:258–264. https://doi.org/10.1016/j.bios.2012.07.034

Ravalli A, Santos GP, Ferroni M, Faglia G, Yamanaka H, Marrazza G (2013) New label free CA125 detection based on gold nanostructured screen-printed electrode. Sens Actuators B Chem 179:194–200. https://doi.org/10.1016/j.snb.2012.10.017

Sanzó G, Taurino I, Antiochia R, Gorton L, Favero G, Mazzei F, Micheli GD, Carrara S (2016) Bubble electrodeposition of gold porous nanocorals for the enzymatic and non-enzymatic detection of glucose. Bioelectrochemistry 112:125–131. https://doi.org/10.1016/j.bioelechem.2016.02.012

Scholler N, Urban N (2007) CA125 in ovarian cancer. Biomark med 1:513–523. https://doi.org/10.2217/17520363.1.4.513

Schramm C, Binder WH, Tessadri R (2004) Durable press finishing of cotton fabric with 1,2,3,4-butanetetracarboxylic acid and TEOS/ GPTMS. J Solgel Sci Technol 29:155–165. https://doi.org/10.1023/B:JSST.0000

Schumann C, Taratula O, Khalimonchuk O, Palmer AL, Cronk LM, Jones CV, Escalamte CA, Taratula O (2015) ROS-induced nanotherapeutic approach for ovarian cancer treatment based on the combinatorial effect of photodynamic therapy and DJ-1 gene suppression. Nanomed-nanotechnol 11:1961–1970. https://doi.org/10.1016/j.nano.2015.07.005

Singh P, Pandit S, Mokkapati VRSS, Garg A, Ravikumar V, Mijakovic I (2018) Gold nanoparticles in diagnostics and therapeutics for human cancer. Int J Mol Sci 19:1–8. https://doi.org/10.3390/ijms19071979

Tian Y, Liu H, Zhao G, Tatsuma T (2006) Shape-controlled electrodeposition of gold nanostructures. J Phys Chem B 110:23478–23481. https://doi.org/10.1021/jp065292q

Torre LA, Trabert B, DeSantis CE, Miller KD, Samimi G, Runowicz CD, Gaudet MM, Jemal A, Siegel RL (2018) Ovarian cancer statistics, 2018. CA Cancer J Clin 68:284–296. https://doi.org/10.3322/caac.21456

Ueland FR (2017) A perspective on ovarian cancer biomarkers: past, present and yet-to-come. Diagnostics (Basel, Switzerland) 7(1):Pii: E14 https://doi.org/10.3390/diagnostics7010014. https://www.ncbi.nlm.nih.gov/pubmed/28282875

Wang C, Zhang Y, Dong L, Fu L, Bai Y, Li T, Xu J, Wei Y (2000) Two-dimensional ordered arrays of silica nanoparticles. Chem Mater 12:3662–3666. https://doi.org/10.1021/cm990738j

World Health Organization (2019) 066 Population Fact Sheets. Global Cancer Obervatory, Pakistan

Yina Y, Huang R, Xu Y, Wang C (2017) Preparation and characterization of highly dispersed silica nanoparticles via nonsurfactant template for fabric coating. J Text I 108:1662–1668. https://doi.org/10.1080/00405000.2017.1278999

Zhong G, Lan R, Zhang W, Fu F, SunY PH, Chen T, Cai Y, Liu A, Lin J, Lin X (2015) sensitive electrochemical immunosensor based on three-dimensional nanostructure gold electrode. Int J Nanomedicine 10:2219–2228. https://doi.org/10.2147/IJN.S76200

Zhu Z, Shi L, Feng H, Zhou HS (2015) Single domain antibody coated gold nanoparticles as enhancer for Clostridium difficile toxin detection by electrochemical impedance immunosensors. Bioelectrochemistry 101:153–158. https://doi.org/10.1016/j.bioelechem.2014.10.003